Inelastic multiphonon helium scattering from a stepped Ni(977) surface

Daniel J. Gaspar, Aubrey T. Hanbicki, and S. J. Sibener[a)]
The James Franck Institute and Department of Chemistry, University of Chicago, Chicago, Illinois 60637

(Received 19 May 1998; accepted 21 July 1998)

The multiphonon energy exchange between a neutral He atom and a stepped Ni(977) surface has been measured in order to examine how the presence of a regular array of atomic-scale steps on a surface modifies energy exchange in the classical multiphonon scattering regime. At elevated substrate temperatures, we compare the multiphonon scattering with the predictions of a classical theory that has previously been used by others for assessing energy exchange involving a smooth surface. There is a significant discrepancy between the theoretical predictions and our experimental data, which we attribute to differences between a smooth and stepped surface. Specifically, changes in the vibrational modes and associated surface density of states due to the presence of extended surface defects have a fundamental impact on the details of the energy exchange mechanism. © *1998 American Institute of Physics.* [S0021-9606(98)70640-3]

I. INTRODUCTION

Energy transfer from a gas phase atom or molecule to a solid surface has been the subject of much study because of its importance in energy accommodation, sticking, and other gas–surface phenomena. The details of energy exchange, including angular dependencies and energy and momentum partitioning, can be precisely examined with the use of molecular beam–surface scattering experiments. For instance, experiments using energetic beams of noble gases scattered from single crystal surfaces have been carried out on many metal surfaces to study energy transfer. Some systems studied include He/Cu(001),[1–3] Xe/Ag(100),[4] Xe/Pt(111),[5] Ar/Pt(111),[6,7] and He/Pt(111).[8] Semiconductor surfaces, such as Xe/GaAs(110)[4] and Xe/Ge(100),[4] and dielectric surfaces, such as He/LiF(001)[9] and He/KCN(001),[10] have also been examined. Molecule–single crystal scattering experiments for systems such as H_2/Ag(111),[11] D_2/Ag(111),[11] HD/Ag(111),[11] N_2/Ag(111),[12] N_2/Pt(111),[13] CH_4/Pt(111),[13] and NO/Ag(111)[14] have allowed energy transfer to other degrees of freedom (vibrations and rotations) to be examined. In addition, studies have been performed using a polycrystalline tungsten surface, Ar/W(poly)[15] and N_2/W(poly),[16] although the effects of a regular array of defects cannot be determined from such studies.

The differences in the electronic and vibrational density of states of a surface with defects, as compared to a defect free surface, are well established.[17–19] Studies performed with polycrystalline surfaces provide angular information averaged over different crystal directions and a range of incident angles. Thus, effects due purely to defects are difficult to extract and the influence of a periodic array of defects on energy transfer is not known. To this end, a regularly stepped surface offers a model system to explore these issues.

Our understanding of the details of the dynamics of energy transfer continues to undergo refinement. For model systems, such as noble gas atoms and weakly corrugated metal surfaces, several theories have shown agreement with some or all aspects of energy and momentum transfer. Early models for energy exchange include the hard cube model,[20] which assumes parallel momentum conservation, i.e., $\Delta \mathbf{K} = 0$. The exchange takes the form of an impulsive collision in the z direction only. This model gives qualitative (and in some cases quantitative) agreement for several systems, although generally only systems involving heavier noble gases such as Xe, Kr, or Ar.[21,22]

Another method, first developed by Adelman and Doll[23–27] and later refined by Tully,[28–30] uses a bath-system separation of variables to reduce the dimensionality of the system. The classical generalized Langevin equation (GLE) formalism is used to treat a bath of phonons driven by collision with gas atoms or molecules. Stochastic classical trajectories are run by numerically integrating the (now reduced) equations of motion. This method requires the potential energy surface for the interaction between the gas atom and the surface to be known very accurately; this is a problem for many systems (including He/Ni(977)). In addition, a friction force and a random fluctuating force must be constructed to reproduce the appropriate surface dynamics. This method has been used on a variety of systems and has shown good agreement with several different experiments.[28–34]

Jackson has recently reported[35] a reduced density matrix method which treats the bath phonons and the particle evolution rigorously. However, surface structure is ignored. In addition, the bath dynamics are assumed to be Markovian, i.e., the time scale for bath relaxation is much shorter than the particle interaction time. At higher collision energies, and shorter collision times, such as in our experiment, this assumption may not be valid.

We have chosen a theory developed by Manson, Celli, and Himes[36,37] to compare with our experiment. The theory has been successfully applied to several systems,[38–47] and recent work on the He/Cu(001)[1–3] system shows excellent agreement in all aspects of the multiphonon energy exchange, including mean energy exchange, angular depen-

[a)]Electronic mail: s-sibener@uchicago.edu

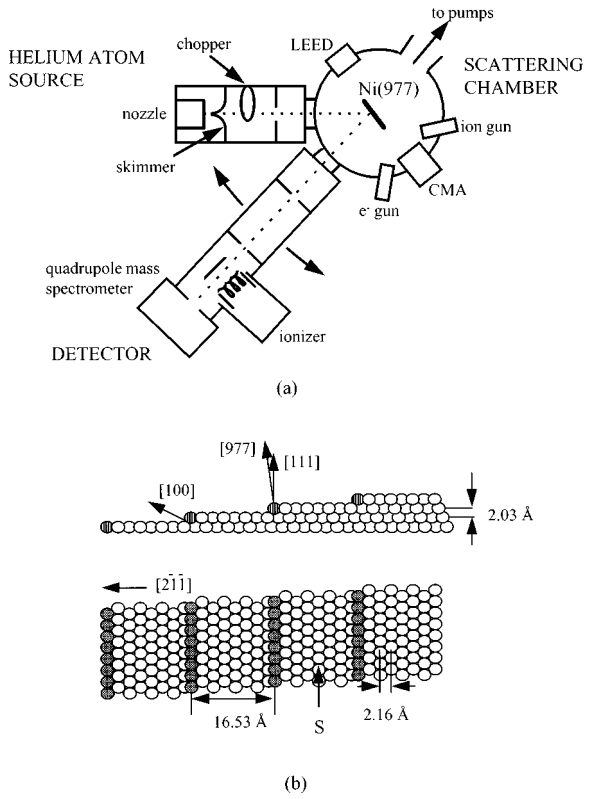

FIG. 1. A schematic of the high resolution helium scattering machine is shown in (a). The monoenergetic helium atom source is on the left, the scattering chamber is in the upper right, and the rotatable quadrupole mass spectrometer is on the bottom. Top and side views of the Ni(977) surface are depicted in (b). The scattering plane contains the normal to the (111) terraces, and the scattering direction, *S*, is parallel to the steps. In both views, atoms located at the step are shaded.

dence, temperature dependence, and linewidth. In addition, for the He/Cu(001) system, the temperature dependence of the multiphonon intensity clearly distinguishes between two forms of the theory. Since the He/Cu(001) interaction is similar to the He/Ni(111) interaction, we expected qualitatively similar behavior for the Ni(977) surface (the majority of which is composed of Ni(111) terraces), although it is reasonable to expect that the presence of the steps, and hence the modified surface vibrational and electronic density of states, may alter the energy exchange behavior. The temperature dependence for scattering from a stepped surface may also differ, as is examined in detail in Sec. V. This experiment, therefore, provides a test of two key aspects of the scattering theory: the influence of extended defects and the temperature dependence of energy accommodation.

II. EXPERIMENT

These experiments were carried out in our high momentum- and energy-resolution helium atom scattering apparatus. The helium scattering instrument has been described elsewhere,[48] but a brief review is given here. The instrument essentially consists of three main parts: a supersonic helium beam source, an UHV scattering chamber equipped with appropriate surface characterization tools, and a rotating, long flight path, quadrupole-based detector. A schematic is shown in Fig. 1(a).

The supersonic nozzle source has three differentially pumped regions. The first region contains the variable temperature nozzle; in these experiments a 20 μm Mo pinhole, and an electroformed skimmer. The second region contains a chopper wheel for time-of-flight (TOF) measurements, rotating in these experiments at 100 Hz with four timing slits. The third region is a buffer region to reduce the gas load in the scattering chamber. Ultrahigh purity helium (99.999%) was used at a backing pressure of 300 psi; the incident beam energy could be selected by tuning the nozzle temperature. The experiments reported here were performed with a 63 meV beam. For the current configuration, we have measured a $\Delta v/v$ of 3.5%, corresponding to an energy resolution of about 4.4 meV for a 63 meV beam.

The scattering chamber is pumped by diffusion, Ti sublimation, cryo and ion pumps. Sample heating is provided by Mo button heaters mounted on the rear of the sample plate. A two-stage closed-cycle helium refrigerator provides sample cooling via a copper braid. A base pressure of 7×10^{-11} Torr is routinely achieved. While scattering in the TOF mode, the scattering chamber pressure rises to about 2.0×10^{-10} Torr. The sample is mounted on a three-axis manipulator with polar, azimuth, and tilt capabilities. The manipulator is mounted off center on a large rotatable lid, so that the sample can be positioned in front of surface characterization and cleaning instruments such as LEED, a double-pass cylindrical mirror analyzer for Auger electron spectroscopy, and a sputter ion gun.

Scattered helium atoms are ionized by electron bombardment and detected with a quadrupole mass spectrometer. The detector is triply differentially pumped with a He base pressure in the ionizer region on the order of 1×10^{-14} Torr. The entire detector is mounted on a rotatable arm with an angular range of $\pm20°$. This arrangement allows measurement of a range of final scattering states for a given initial condition [see Fig. 1(a)]. Rotation is performed under computer control with an optical encoder providing the relative accuracy of $\pm0.02°$, with an absolute accuracy of less than $\pm0.4°$. The chopper-to-crystal distance is 55.1 cm and the chopper-to-ionizer distance, the effective total flight path, is 156.6 cm.

The sample used in these studies is a Ni(977) crystal prepared by the Princeton Scientific Corp. The Ni(977) surface [shown schematically in Fig. 1(b)] is prepared by cutting a Ni single crystal 7.02° from the (111) plane in the [211] direction. Laue x-ray backreflection was used to confirm crystal orientation to better than 0.5°. The surface consists of eight atom wide (111) terraces separated by monatomic (100) steps. Alternatively, the surface can be labeled using microfacet notation as Ni[$8(111)\times(100)$]. The sample was cleaned by repeated cycles of sputtering with 1 kV Ar^+ atoms with the surface held at 1000 K followed by annealing above 1030 K until C and S levels were below our Auger detection limit. A sharp LEED pattern with splitting of half of the (111) spots (characteristic of the stepped surface) confirmed surface crystallinity. Experiments were carried out in the temperature range of 700–1000 K and all were carried in out in the TOF mode, allowing us to energy resolve and isolate the multiphonon and elastic intensities.

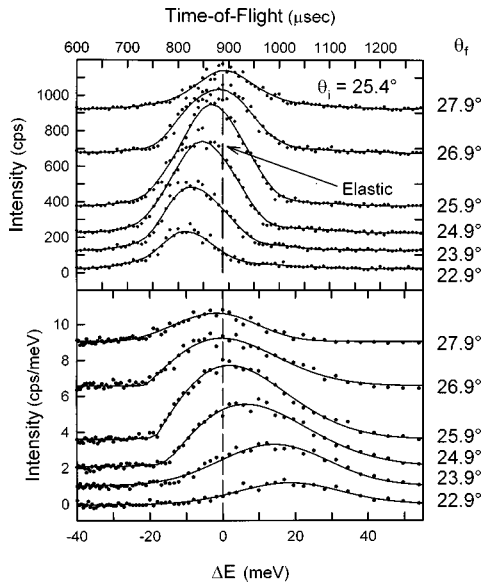

FIG. 2. Top panel: Six representative TOF spectra (filled circles) taken at $T_s = 1000$ K with a smoothed line as a guide to the eye. Each spectrum was taken under the same initial conditions ($E_i = 63$ meV, $\theta_i = 25.4°$) with different final angles, as indicated in the figure. The scattering kinematics are out-of-phase, i.e., anti-Bragg conditions, with respect to the steps height between adjacent terraces. The elastic flight time is 888 μs. Bottom panel: Energy transfer spectra (filled circles) calculated from spectra in the top panel. The solid line is a guide to the eye.

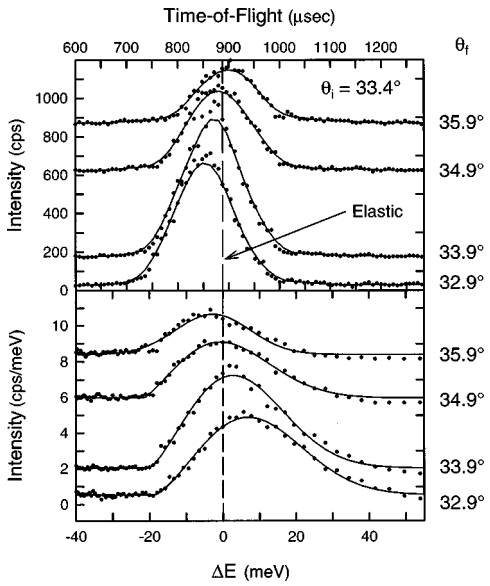

FIG. 3. Top panel: Four representative TOF spectra (filled circles) taken at $T_s = 1000$ K with a smoothed line as a guide to the eye. Each spectrum was taken under the same initial conditions ($E_i = 63$ meV, $\theta_i = 33.4°$) with different final angles. The scattering kinematics are in phase, i.e., Bragg conditions, with respect to the step height between adjacent terraces. The elastic flight time was 888 μs. Bottom panel: Energy transfer spectra (filled circles) calculated from spectra in the top panel. The solid line is a guide to the eye.

During a series of TOF measurements, no signal degradation occurred, and Auger measurements performed at the end of a series of measurements showed no measurable surface contamination. A reference spectrum was taken at $T_s = 1000$ K at the beginning of each day to normalize small changes in the scattered intensity and elastic flight time.

III. RESULTS

The top panel in Fig. 2 shows TOF data, taken using 8 μs/channel dwell periods for $\theta_i = 25.4°$ and $T_s = 1000$ K. The bottom panel of Fig. 2 shows the corresponding energy transfer spectra. All data presented in this work were collected using a room temperature beam, corresponding to an incident helium atom energy of 63 meV. Six representative final angles are shown. At final angles further than three degrees from specular, the multiphonon signal decreases to the level of the background. The elastic flight time is indicated by a dashed vertical line. Figure 3 contains four representative TOF and energy transfer spectra (top and bottom panels, respectively) for the other initial angle studied, $\theta_i = 33.4°$, at $T_s = 1000$ K, with the elastic flight time again shown as a vertical dashed line.

The scattering kinematics were chosen so that the incident wave vector was nominally out-of-phase (anti-Bragg scattering) or in-phase (Bragg scattering) with respect to the step height between adjacent terraces. The out-of-phase condition is $\theta_i = 25.4°$, and the in-phase condition is $\theta_i = 33.4°$. Since multiphonon scattering is typically incoherent, we did not expect to see any differences in the two conditions as a result of the phase condition, and, indeed, no difference was seen. The same behavior was observed for the multiphonon energy transfer peaks for both initial conditions and all surface temperatures. Therefore, although all of the data have been analyzed in detail, for the rest of this work we will present only analyses for data taken at the out-of-phase condition.

For a given temperature, when the TOF signal for each final angle is integrated, the resulting angular plots are equivalent to diffraction spectra. Figure 4 shows the resulting diffraction spectra as a function of surface temperature for all TOF spectra taken in the out-of-phase condition. For the

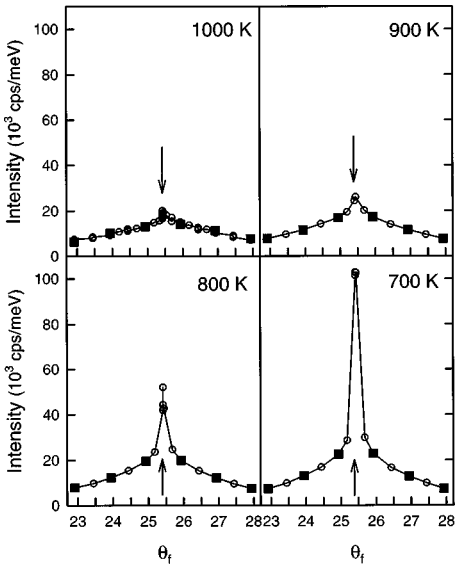

FIG. 4. Integrated TOF as a function of angle. The filled squares are the data shown in Fig. 2 and used to compare with the theory in the remainder of this paper. The arrow in each panel indicates the specular angle. For all spectra used to generate these plots, $\theta_i = 25.4°$ and $E_i = 63$ meV.

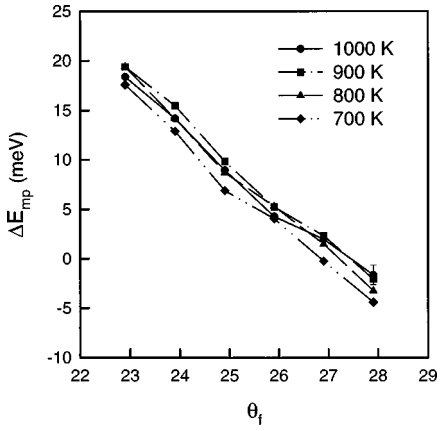

FIG. 5. The most probable energy transfer (multiphonon peak position) as a function of the final angle shown for $T_s = 700$ K–1000 K.

1000 K data, the filled squares are the TOF spectra shown in the top panel of Fig. 2. The coherent specular beam is clearly visible, even at the highest surface temperature, and increases in intensity as the surface temperature is lowered. It is important to analyze only spectra that have no coherent component; Fig. 4 allows us to choose spectra satisfying this requirement.

Each of the energy transfer spectra in the bottom panels of Figs. 2 and 3 exhibits a broad peak centered away from $\Delta E = 0$. For final angles less than $\pm 0.2°$ away from specular, a weak diffuse elastic peak is present in the TOF spectra. Final angles farther than $\pm 0.2°$, however, have no diffuse elastic or single phonon peaks; only the multiphonon background is present. This is consistent with other low-energy helium beam diffraction measurements of the specular diffraction peak (even at 1000 K), which found an angular width of approximately 0.2°.[49]

We now examine the multiphonon background. The intensity of the multiphonon peak decreases quickly as the final angle is moved away from the specular direction. As mentioned previously, at final angles greater than $\pm 3°$ from specular, the multiphonon signal is reduced to the level of the noise. The behavior of the most probable energy transfer (multiphonon peak position) as a function of both the final scattering angle and surface temperature is shown in Fig. 5. With increasing the final angle, the most probable energy transfer decreases monotonically from approximately 17–20 meV to -1 to -4 meV, i.e., creation events begin to dominate at wide angles. We estimate an upper bound on the error in the most probable energy transfer to be 1 meV, shown by a representative error bar on the 1000 K data. Within the limit of this error, no consistent change in the most probable energy transfer as a function of temperature is noted.

IV. REVIEW OF THEORY

The theory of inelastic multiphonon scattering developed by Manson, Celli, and Himes has recently been summarized elsewhere.[36,50] In this section we highlight some of the salient features of this theory. We have used the classical scattering version of this theory, as developed within the trajectory approximation. Justification for the use of classical scattering as a model for the gas–surface interaction of our system is based on the relatively high energy of the collisions under study.

TABLE I. Debye–Waller exponents, $2W$, for both Bragg and anti-Bragg incident conditions, as a function of the surface temperature. For $2W > 6$, classical scattering is considered a good approximation.

θ_i	θ_f	$2W\ (T_s)$	1000 K	900 K	800 K	700 K
25.4	22.9		8.8	7.9	7.1	6.2
	27.9		8.5	7.6	6.8	5.9
33.4	30.4		7.6	6.9	6.1	5.3
	36.4		7.1	6.4	5.7	5.0

Previous work has suggested that classical behavior becomes important when the Debye–Waller exponent, $2W$, is larger than 4 and should dominate for $2W \geqslant 6$.[50] The Debye–Waller exponent can be calculated, assuming a Debye model for the phonon spectrum, using

$$2W(\Delta\mathbf{k}) = \frac{3\hbar^2\ \Delta\mathbf{k}^2\ T_s}{M_s k_b \Theta_D^2}, \tag{1}$$

where M_s is the surface atom mass, T_s is the surface temperature, $\Delta\mathbf{k}$ is the momentum change of the gas atom, and Θ_D is the Debye temperature. Within the Debye model for the phonon spectrum, the Debye–Waller exponent is an estimate of the average number of phonons exchanged in a collision. The $2W$ values for the conditions of this experiment are found in Table I. From these values it is apparent that nearly all of the kinematic conditions used in this study fall within the classical regime. Note that data for surface temperatures below 700 K are not presented in this paper, as this is the regime where quantum contributions become more important, i.e., $2W < 6$. No single-phonon or diffuse elastic peaks are observed in the TOF spectra, leading us to attribute the observed intensities to the multiphonon energy exchange.

Within the classical approximation, the theory can take two forms, depending upon the surface behavior. For a surface that behaves as a smooth continuum (hereafter called the ''continuum'' model), the differential reflection coefficient (i.e., the fraction of particles scattered into a final solid angle $d\Omega_f$ and a final energy dE_f) takes the form

$$\frac{dR}{d\Omega_f\ dE_f} = \frac{m_g^2 |\mathbf{k}_f| v_R^2}{4\pi^3\hbar^5 k_{iz} S_{\text{u.c.}}} |\tau_{fi}|^2 \left(\frac{\hbar^2\pi}{\Delta E_0\ k_b T_s}\right)^{3/2} \times \exp\left(-\frac{(\Delta E + \Delta E_0)^2 + 2\hbar^2 v_R^2 \Delta\mathbf{K}^2}{4k_b T_s \Delta E_0}\right). \tag{2}$$

For a surface whose potential arises from a collection of discrete scattering centers (hereafter referred to as the ''discrete'' model), the reflection coefficient takes the form

$$\frac{dR}{d\Omega_f\ dE_f} = \frac{m_g^2 |\mathbf{k}_f|}{8\pi^3\hbar^5 k_{iz}} |\tau_{fi}|^2 \left(\frac{\hbar^2\pi}{\Delta E_0\ k_b T_s}\right)^{1/2} \times \exp\left(-\frac{(\Delta E + \Delta E_0)^2}{4k_b T_s\ \Delta E_0}\right). \tag{3}$$

In these equations, m_g is the gas particle mass, $|\mathbf{k}_f|$ is the magnitude of the final gas particle momentum, v_R is a char-

acteristic phonon velocity, k_{iz} is the perpendicular component of the gas particle momentum, $S_{\text{u.c.}}$ is the unit cell area, τ_{fi} is a scattering matrix element, ΔE_0 is the recoil energy of an individual surface atom, T_s is the surface temperature, ΔE is the energy exchange, and $\Delta \mathbf{K}$ is the parallel momentum exchange. ΔE_0, the recoil energy of an individual surface atom, is given by

$$\Delta E_0 = \frac{\hbar^2 \, \Delta \mathbf{k}^2}{2M_s}, \tag{4}$$

where $\Delta \mathbf{k}$ is the momentum change and M_s is the mass of a surface atom.

In both of these forms, we can think of the reflection coefficient as consisting of four parts: (1) a temperature-independent prefactor, (2) matrix element, (3) temperature-dependent prefactor, and (4) a Gaussian-type function. Note that the Debye–Waller factor does not appear explicitly in the theory. The temperature-independent prefactor contains some constants, kinematic factors (k_{iz} and $\mathbf{k}_f$) and, in the continuum model, a v_{R}^2 term. The characteristic phonon velocity, v_{R}, accounts for correlated vibrations in the solid and should be of the same order as the Rayleigh wave velocity (since these modes should dominate the energy transfer). Note that since the presence of the phonon velocity arises from correlated vibrations, the discrete model contains no v_{R} factor. The transition matrix amplitude, τ_{fi}, was chosen to be of the same form as Hofmann *et al.*,[3] and is resolved into a product of parallel and perpendicular components. The parallel component is a Gaussian cutoff function, while the perpendicular component is a Mott–Jackson matrix element (see, for example, Goodman and Wachman[20]):

$$\tau_{fi} = e^{-\Delta \mathbf{K}^2/2Q_c^2} \nu_{\text{M–J}}. \tag{5}$$

Here, $\Delta \mathbf{K}$ is the parallel momentum transfer, Q_c is a parallel momentum cutoff parameter,[43] and the Mott–Jackson matrix element, $\nu_{\text{M–J}}$, is calculated for an exponentially repulsive potential of the form $\exp(-\beta z)$. Both the steepness of the repulsive potential, β, and parallel momentum cutoff, Q_c, are used as adjustable parameters. The form of the transition matrix element is the same for both the continuum and discrete models.

The third term, the temperature-dependent prefactor, contains the fundamental difference between the two models. In particular, the temperature dependence of the reflection coefficient is $T^{-3/2}$ for the continuum model and $T^{-1/2}$ for the discrete model. The temperature dependence of the multiphonon scattering intensity should therefore distinguish between the two forms of the gas–surface scattering theory. Work on Cu(001) showed excellent agreement with the continuum model,[1,3] so the similarity between Ni and Cu might lead one to expect that the continuum model would also adequately describe the energy exchange for He/Ni(977). However, the Ni(977) surface contains a regular array of steps, with associated differences in the surface density of vibrational states and the surface's electronic band structure. It is possible that the stepped surface is described more appropriately as a discrete lattice, leading to a temperature dependence that varies from $T^{-3/2}$.

The fourth term, the Gaussian-type function, contains two interesting variables. One, the recoil energy ΔE_0, serves as the energy scale for the multiphonon energy exchange predicted by this theory. The other variable, v_{R}, is found only in the continuum model, where an additional term containing v_{R}^2 serves to add additional width to the multiphonon peak. Because this term scales as $|\Delta \mathbf{K}|^2$, for the small parallel momentum transfer observed in these experiments it is negligible.

The interaction potential used to calculate scattering matrix elements is a purely repulsive potential. However, a realistic He/Ni(977) potential has an attractive portion that accelerates the incoming atom toward the surface. The well-known ''Beeby correction'' [51] accounts for this by adding an amount of energy equal to the well depth near the surface in the direction perpendicular to the gas particle. The He/Ni(110) attractive well depth has been found to be 4.2 meV.[52] Because the attractive well depth of He/metal(111) potentials are typically 1–2 meV higher than that of He/metal(110) potentials,[52] we estimate D to be 6 meV for the He/Ni(111) system. For a helium atom with an incident energy of 63 meV, this amount becomes significant. Jackson reported a study of the one-phonon molecule surface scattering using a Gaussian wave packet approach, where the Beeby correction appeared to be invalid.[53] In that work, the energy transfer did not scale with perpendicular energy, so no simple correlation between the well depth and the energy exchange was found. For multiphonon excitation, as in the experiment presented here, the perpendicular component of the incident energy *should* affect the energy transfer. As is evident from Eqs. (2) and (3), the incident perpendicular momentum appears explicitly, as does the final momentum vector. Additionally, the matrix elements have initial and final momentum as well as angle dependencies. The Beeby correction should, therefore, be a necessary and valid approximation for this experiment. Accordingly, we have included a Beeby correction in all calculations, although changes in the behavior of the theory due to the Beeby correction are small.

V. ANALYSIS

We can use the theory just reviewed to calculate our energy transfer spectra and examine the temperature behavior of the multiphonon spectra. To fit the calculated energy transfer spectra to the experimental data, an intensity (scaling) parameter was used as well as the following previously discussed quantities: v_{R}, Q_c, and β. The intensity parameter serves to normalize the predicted final flux with respect to the experimental incident flux. Accordingly, the intensity parameter should ideally be fixed at a single value for all conditions. This leads to poor agreement with the measurements. Therefore, we allowed the intensity parameter to change at each final angle, though it was fixed as a function of temperature.

Previously, multiphonon energy exchange on Cu(001) has been fit using a v_{R} value of 3000 m/s[3] and on Pt(111), with v_{R} values of 1900[8] and 1$\underline{2}$34 m/s.[54] The Rayleigh wave velocity for Ni(111) (near the $\bar{\Gamma}$ point) has been measured to be 425 m/s by Stirniman *et al.*[55] For Ni(977), the calculated

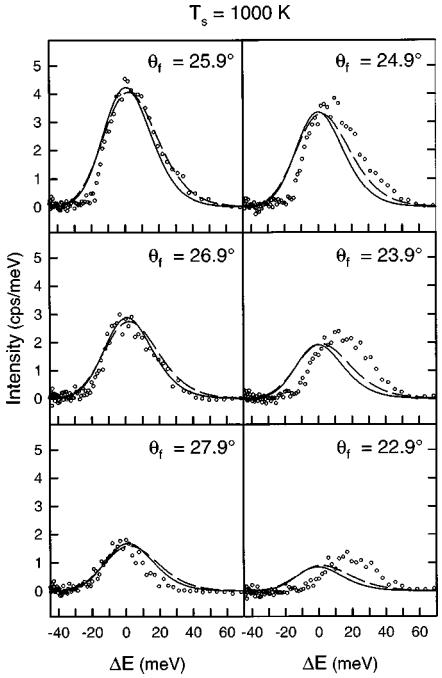

FIG. 6. Six energy transfer spectra (open circles), with continuum model fits (solid lines), and discrete model fits (dashed lines), taken at $T_s = 1000$ K. The incident angle, θ_i, is 25.4° for each spectrum and the incident energy is 63 meV. The parameters used to generate the continuum model fits were the following: $\beta = 2.9$ Å^{-1}, $Q_c = 3.2$ Å^{-1}, $v_R = 2500$ m/s. The discrete model fits were the following: $\beta = 3.4$ Å^{-1}, $Q_c = 2.2$ Å^{-1}.

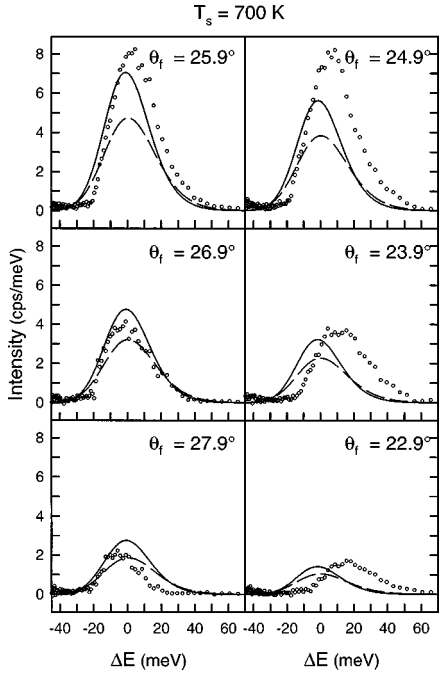

FIG. 7. Six energy transfer spectra (open circles), with predictions generated from the continuum model (solid lines) and discrete model (dashed lines) at $T_s = 700$ K. The incident angle, θ_i, is 25.4° for each spectrum and the incident energy is 63 meV. The parameters used to generate the theoretical spectra were those determined at 1000 K.

multiphonon energy exchange spectrum exhibits minimal dependence on variations in the v_R parameter from 100 to 5000 m/s. Accordingly, this parameter was fixed at 2500 m/s throughout this work.

The remaining two parameters were determined by considering the spectra taken at the six final angles shown in the bottom panel of Fig. 2. A global best fit for fixed values of β and Q_c was obtained using a sum of the goodness of fit parameters determined for each final angle. For the continuum model, the best fit parameters determined in this fashion were $\beta = 2.9$ Å^{-1} and $Q_c = 3.2$ Å^{-1}. Using the discrete model, $\beta = 3.4$ Å^{-1} and $Q_c = 2.2$ Å^{-1}; recall that the discrete form of the theory contains no v_R terms. We note, however, that the fits are not very sensitive to the values of β and Q_c. The results of the theoretical fits using both the continuum and discrete models, along with the experimental data at $T_s = 1000$ K, are shown in Fig. 6. In Figs. 6 and 7, the open circles are the data, the solid lines are the continuum model theoretical spectra, and the dashed lines are the spectra calculated using the discrete model. The two forms of the theory agree equally well at $T_s = 1000$ K because the adjustable parameters are optimized independently for each model in an attempt to fit the 1000 K dataset; it is only when the temperature dependence is analyzed that the models diverge. The results for $T_s = 700$ K, the lowest temperature studied, are shown in Fig. 7. In general, the peak shape and width are well reproduced, although the predicted peak position (the most probable energy loss) does not show agreement for some conditions.

Using the parameters obtained above, we now examine the temperature dependence of the multiphonon intensity and compare the two forms of the theory. As discussed in the Introduction, the discrete model has a $T^{-1/2}$ intensity envelope while the continuum model intensity goes as $T^{-3/2}$. The procedure for comparing the temperature dependence of the data to the two forms of the theory is as follows: (1) best fit parameters were determined for both forms of the theory using the data taken at 1000 K; (2) all parameters were fixed for surface temperatures lower than 1000 K; (3) the goodness of fit parameters of the two forms of the theory were compared as a function of temperature.

The results of this comparison are shown in Fig. 8 for two illustrative final angles, $\theta_f = 24.9°$ (left column) and $\theta_f = 25.9°$ (right column). The data at these angles most clearly demonstrate the temperature dependence of the multiphonon intensity. At angles farther from specular, the capacity of the data to distinguish between the two forms of the theory is minimal. Each panel in Fig. 8 contains four spectra, one at each of the four surface temperatures studied. The experimental spectra are shown in the top row of panels. Spectra calculated using the continuum model are shown in the middle row of panels, while the bottom row of panels contains the discrete model spectra. From this figure, it is evident the continuum model follows the measured trend more closely, i.e., a $T^{-3/2}$ intensity dependence gives a somewhat better prediction of the experimental results. We stress that the temperature-dependent ''fits'' (at $T_s < 1000$ K) are made with no free parameters.

The theory thus far adequately explains the line shape and, to some extent, the temperature dependence of the multiphonon energy transfer. It does not, however, explain the

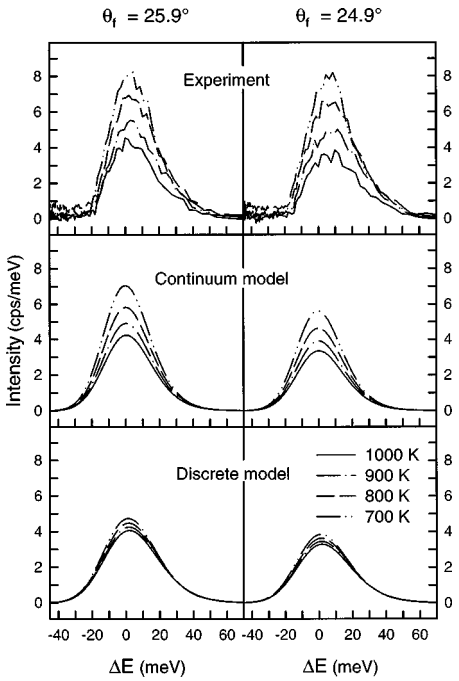

FIG. 8. Temperature dependence of energy transfer calculated from continuum (middle row) and discrete (bottom row) models compared to experiment (top row) for two final angles, $\theta_f = 25.9°$ (left column) and $\theta_f = 24.9°$ (right column). The data at these angles most clearly demonstrates the temperature dependence of the multiphonon intensity.

peak position. To understand the origin of this inconsistency, we examine the angular dependence of the final momentum. Figure 9 shows parallel momentum versus perpendicular momentum for spectra (filled symbols) taken at six final angles and the four surface temperatures studied. Also shown (lines) are the momenta predicted by the theory. The prediction of a simple hard cube model is also shown (hollow circles). The main feature of the hard cube model is $\Delta\mathbf{K} = 0$, so that it also

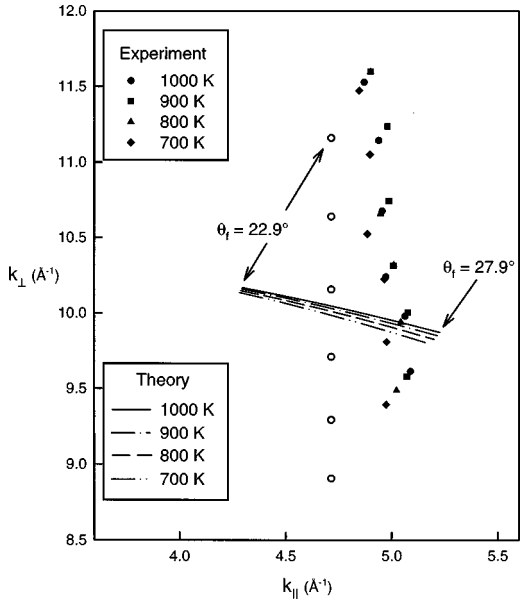

FIG. 9. Perpendicular versus parallel momentum, for experiment (filled symbols), continuum model of theory (lines), and a simple hard cube model (open circles).

serves in Fig. 9 as a convenient reference. Clearly, the data and the theory disagree as to the partitioning of momentum into parallel and perpendicular components. On the one hand, the theory predicts a large change in parallel momentum as a function of the final angle; the parallel momentum increases from 4.3 to about 5.2 $Å^{-1}$, as the final angle is increased from 22.9° to 27.9°, while the corresponding decrease in perpendicular momentum is very small, approximately 0.3 $Å^{-1}$. On the other hand, our experiment shows that parallel momentum is nearly conserved, increasing only by 0.1–0.2 $Å^{-1}$. Additionally, the measured perpendicular momentum decreases with increasing final angle by approximately 1.0 $Å^{-1}$. In other words, nearly all the energy transfer occurs in the perpendicular coordinate. Upon examination of Figs. 6 and 7, theory and experiment appear to show better agreement for supra-specular angles than for subspecular angles. Figure 9 clearly shows that this is a coincidence arising from the intersection of the momentum partitioning curves derived from experiment and theory. The experimental curves are closer to the calculated curves for the supraspecular final angles used in this experiment than for the subspecular final angles.

VI. DISCUSSION

The disagreement between theory and experiment may arise from several sources. First, this theory is only suitable for experimental conditions that are essentially classical. Quantum and semiclassical theories do exist for conditions where quantum scattering contributes to the energy exchange;[35,50,53] however, under the experimental conditions reported here, classical scattering should be an excellent approximation, even at 700 K. As mentioned in Sec. IV, Debye–Waller exponents, $2W$, corresponding to six or more phonons exchanged on average in each collision should ensure that quantum mechanical effects are averaged out (see Table I). In addition, we see no evidence for single phonon or diffuse elastic scattering in the TOF spectra. Therefore it is unlikely that quantum mechanical effects are the cause of the observed disagreement between experiment and theory.

Another possibility could be that the origin of the observed intensity is not multiphonon exchange, but rather is due to surface (or step) roughening. The effect of a rough surface is to average over different impact parameters, leading to enhanced *elastic* signal at off-specular angles. Our energy-resolved spectra rule out roughening as the source of the scattering signal because no elastic signal is seen at off-specular angles. In addition, other work on this system has demonstrated that no roughening occurs, at least up to the temperatures studied.[49]

In light of the excellent agreement between this theory and other experiments on low Miller index surfaces, we look to the presence of the steps to explain our observations. In particular, the electronic and vibrational structure and density of states near a step are modified from that of a flat surface.[17,56–64] The electronic density of states near a step exhibits Friedel oscillations. The potential near the steps, therefore, should reflect this behavior and may have a significant impact upon the scattering process. However, under

the conditions of this experiment, the energy exchange should be insensitive to small deviations of this type.

Previous work has shown that the dominant phonons in multiphonon energy exchange are the low-energy Rayleigh modes.[40] On this stepped surface, however, two other low-energy modes have been measured and identified as phonons localized at the step,[56,57] with additional insight coming from related theoretical calculations.[63,64] These are optical modes with behavior away from the Brillioun zone center very similar to the surface Rayleigh mode. Near the zone center (at small parallel momentum transfer), though, the energy of each observed mode deviates from the Rayleigh mode, so that at $\Delta\mathbf{K}=0$, where the Rayleigh mode goes to zero, the step modes still have energies of about 5 and 7 meV. These phonon modes are therefore easily accessible during inelastic collisions of a 60 meV He atom and the surface. In addition, the step localized optical modes have appropriate polarizations[63,64] for collisionally induced energy transfer, with nonzero projections along the surface normal.[56,57] Thus, significant energy transfer can even occur during collisions with little or no parallel momentum transfer, a condition unique to this stepped surface.

VII. SUMMARY

Multiphonon energy transfer has been studied on a stepped nickel surface using high-resolution helium atom scattering. The experimental conditions have been chosen to be in a regime where the scattering is expected to behave in an essentially classical manner. The temperature and angular dependence of the scattered multiphonon intensity has been compared to existing theory, used previously under similar conditions to successfully describe the details of the multiphonon energy exchange for helium scattered from Cu(001). For helium scattered from stepped nickel, the temperature dependence of the experimental multiphonon intensity shows somewhat better agreement with one form of the theory, the continuum model. However, a global examination of the data reveals significant disagreement between theory and experiment, i.e., the momentum partitioning shows behavior deviating from the predictions of the theory. The presence of step-localized optical phonon modes may account for this discrepancy.

ACKNOWLEDGMENTS

The authors would like to thank Professor J. R. Manson for many helpful discussions about the theory. Funding for this work was provided by the AFOSR and the NSF-MRSEC (Award No. DMR-9400379) at the University of Chicago.

[1] F. Hofmann, J. P. Toennies, and J. R. Manson, J. Chem. Phys. **106**, 1234 (1997).
[2] F. Hofmann, J. P. Toennies, and J. R. Manson, J. Chem. Phys. **101**, 10 155 (1994).
[3] F. Hofmann, J. P. Toennies, and J. R. Manson, Surf. Sci. **349**, L184 (1996).
[4] A. Amirav, M. J. Cardillo, P. L. Trevor, C. Lim, and J. C. Tully, J. Chem. Phys. **87**, 1796 (1987).
[5] J. E. Hurst, C. A. Becker, J. P. Cowin, K. C. Janda, L. Wharton, and D. J. Auerbach, Phys. Rev. Lett. **43**, 1175 (1979).
[6] J. E. Hurst, L. Wharton, K. C. Janda, and D. J. Auerbach, J. Chem. Phys. **78**, 1559 (1983).
[7] J. E. Hurst, L. Wharton, K. C. Janda, and D. J. Auerbach, J. Chem. Phys. **83**, 1376 (1985).
[8] V. Celli, D. Himes, P. Tran, J. P. Toennies, C. Wöll, and G. Zhang, Phys. Rev. Lett. **66**, 3160 (1991).
[9] G. G. Bishop, E. S. Gillman, J. Baker, J. J. Hernández, S. A. Safron, J. G. Skofronick, S. M. Weera, and J. R. Manson, Phys. Rev. B **52**, 13 229 (1995).
[10] S. M. Weera, J. R. Manson, J. Baker, E. S. Gillman, J. J. Hernández, G. G. Bishop, S. A. Safron, and J. G. Skofronick, Phys. Rev. B **52**, 14 185 (1995).
[11] K. B. Whaley, C. F. Yu, C. S. Hogg, J. C. Light, and S. J. Sibener, J. Chem. Phys. **83**, 4235 (1985).
[12] A. C. Kummel, G. O. Sitz, R. N. Zare, and J. C. Tully, J. Chem. Phys. **91**, 5793 (1989).
[13] K. C. Janda, J. E. Hurst, J. P. Cowin, L. Wharton, and D. J. Auerbach, Surf. Sci. **130**, 395 (1983).
[14] J. Kimman, C. T. Rettner, D. J. Auerbach, and J. A. Barker, Phys. Rev. Lett. **57**, 2053 (1986).
[15] K. C. Janda, J. E. Hurst, C. A. Becker, J. P. Cowin, D. J. Auerbach, and L. Wharton, J. Chem. Phys. **72**, 2403 (1979).
[16] K. C. Janda, J. E. Hurst, C. A. Becker, J. P. Cowin, L. Wharton, and D. J. Auerbach, Surf. Sci. **93**, 270 (1980).
[17] J. Friedel, Nuovo Cimento Suppl. **7**, 287 (1958).
[18] P. Hofmann, B. G. Briner, M. Doering, H. P. Rust, E. W. Plummer, and A. M. Bradshaw, Phys. Rev. Lett. **79**, 265 (1997).
[19] B. G. Briner, P. Hofmann, M. Doering, H. P. Rust, E. W. Plummer, and A. M. Bradshaw, Europhys. Lett. **39**, 67 (1997).
[20] F. O. Goodman and H. Y. Wachman, *Dynamics of Gas–Surface Scattering* (Academic, New York, 1976).
[21] E. K. Grimmelmann, J. C. Tully, and M. J. Cardillo, J. Chem. Phys. **72**, 1039 (1980).
[22] J. C. Tully, J. Chem. Phys. **92**, 680 (1990).
[23] J. D. Doll and D. R. Dion, J. Chem. Phys. **65**, 3762 (1976).
[24] J. D. Doll and D. R. Dion, J. Chem. Phys. **67**, 3181 (1977).
[25] S. A. Adelman and B. J. Garrison, J. Chem. Phys. **65**, 3751 (1976).
[26] S. A. Adelman and J. D. Doll, J. Chem. Phys. **64**, 2375 (1976).
[27] S. A. Adelman, J. Chem. Phys. **71**, 4471 (1979).
[28] J. C. Tully, J. Chem. Phys. **73**, 1975 (1980).
[29] J. C. Tully, J. Vac. Sci. Technol. **18**, 427 (1981).
[30] J. C. Tully, Faraday Discuss. Chem. Soc. **80**, 291 (1985).
[31] C. Lim, J. C. Tully, A. Amirav, P. Trevor, and M. J. Cardillo, J. Chem. Phys. **87**, 1808 (1987).
[32] R. R. Lucchese and J. C. Tully, J. Chem. Phys. **80**, 3451 (1984).
[33] R. Kosloff and C. Cerjan, J. Chem. Phys. **81**, 3722 (1984).
[34] B. Jackson and H. Metiu, J. Chem. Phys. **83**, 1952 (1985).
[35] B. Jackson, J. Chem. Phys. **108**, 1131 (1998).
[36] J. R. Manson, V. Celli, and D. Himes, Phys. Rev. B **49**, 2782 (1994).
[37] J. R. Manson (private communication, 1997).
[38] R. Brako and D. M. Newns, Phys. Rev. Lett. **48**, 1859 (1982).
[39] R. Brako, Surf. Sci. **123**, 439 (1982).
[40] R. Brako and D. M. Newns, Surf. Sci. **117**, 42 (1982).
[41] M. Persson and J. Harris, Surf. Sci. **187**, 67 (1987).
[42] M. Persson and J. Harris, Surf. Sci. **189/190**, 557 (1987).
[43] V. Celli, G. Benedek, U. Harten, J. P. Toennies, R. B. Doak, and V. Bortolani, Surf. Sci. **143**, L376 (1984).
[44] W. Brenig, Z. Phys. B **36**, 81 (1979).
[45] W. Brenig, Z. Phys. B **36**, 227 (1980).
[46] J. Böheim and W. Brenig, Z. Phys. B **41**, 243 (1981).
[47] R. Sedlmeir and W. Brenig, Z. Phys. B **36**, 245 (1980).
[48] B. Gans, S. F. King, P. A. Knipp, D. D. Koleske, and S. J. Sibener, Surf. Sci. **264**, 81 (1992).
[49] D. J. Gaspar, Ph.D. thesis, University of Chicago, 1998.
[50] J. R. Manson, Nucl. Instrum. Methods Phys. Res. B **96**, 497 (1995).
[51] J. L. Beeby, J. Phys. C **5**, 3438 (1972).
[52] G. Vidali, G. Ihm, H.-Y. Kim, and M. W. Cole, Surf. Sci. Rep. **12**, 133 (1991).
[53] B. Jackson, J. Chem. Phys. **89**, 2473 (1988).
[54] J. R. Manson, Phys. Rev. B **43**, 6924 (1991).
[55] M. J. Stirniman, W. Li, and S. J. Sibener, unpublished work (1994).

[56] L. Niu, D. J. Gaspar, and S. J. Sibener, Science **268**, 847 (1995).
[57] L. Niu, D. D. Koleske, D. J. Gaspar, and S. J. Sibener, J. Chem. Phys. **102**, 9077 (1995).
[58] J. E. Black and P. Bopp, Surf. Sci. **140**, 275 (1984).
[59] G. Armand and P. Masri, Surf. Sci. **130**, 89 (1983).
[60] P. Knipp, Phys. Rev. B **43**, 6908 (1991).
[61] A. Lock, J. P. Toennies, and G. Witte, J. Electron Spectrosc. Relat. Phenom. **54/55**, 309 (1990).
[62] H. Ibach and D. Bruchmann, Phys. Rev. Lett. **41**, 958 (1978).
[63] A. Kara, S. Durukanoglu, and T. S. Rahman, J. Chem. Phys. **106**, 2031 (1997).
[64] E. J. Mele and M. V. Pykhtin, Phys. Rev. Lett. **75**, 3878 (1995).